

Growth Retardation, Impaired Triacylglycerol Catabolism, Hepatic Steatosis, and Lethal Skin Barrier Defect in Mice Lacking Comparative Gene Identification-58 (CGI-58)^{*[5]}

Received for publication, November 3, 2009, and in revised form, December 14, 2009. Published, JBC Papers in Press, December 18, 2009, DOI 10.1074/jbc.M109.081877

Franz P. W. Radner[‡], Ingo E. Streith[‡], Gabriele Schoiswohl[‡], Martina Schweiger[‡], Manju Kumari[‡], Thomas O. Eichmann[‡], Gerald Rechberger[‡], Harald C. Koefeler[§], Sandra Eder[‡], Silvia Schauer[¶], H. Christian Theussl^{||}, Karina Preiss-Landl[‡], Achim Lass[‡], Robert Zimmermann[‡], Gerald Hoefler[¶], Rudolf Zechner^{¶1}, and Guenter Haemmerle^{‡2}

From the [‡]Institute of Molecular Biosciences, University of Graz, Heinrichstrasse 31, A-8010 Graz, the [§]Center for Medical Research and the [¶]Institute of Pathology, Medical University of Graz, A-8010 Graz, and the ^{||}Institute of Molecular Pathology, A-1030 Vienna, Austria

Comparative gene identification-58 (CGI-58), also designated as α/β -hydrolase domain containing-5 (ABHD-5), is a lipid droplet-associated protein that activates adipose triglyceride lipase (ATGL) and acylates lysophosphatidic acid. Activation of ATGL initiates the hydrolytic catabolism of cellular triacylglycerol (TG) stores to glycerol and nonesterified fatty acids. Mutations in both ATGL and CGI-58 cause “neutral lipid storage disease” characterized by massive accumulation of TG in various tissues. The analysis of CGI-58-deficient (*Cgi-58*^{-/-}) mice, presented in this study, reveals a dual function of CGI-58 in lipid metabolism. First, systemic TG accumulation and severe hepatic steatosis in newborn *Cgi-58*^{-/-} mice establish a limiting role for CGI-58 in ATGL-mediated TG hydrolysis and supply of nonesterified fatty acids as energy substrate. Second, a severe skin permeability barrier defect uncovers an essential ATGL-independent role of CGI-58 in skin lipid metabolism. The neonatal lethal skin barrier defect is linked to an impaired hydrolysis of epidermal TG. As a consequence, sequestration of fatty acids in TG prevents the synthesis of acylceramides, which are essential lipid precursors for the formation of a functional skin permeability barrier. This mechanism may also underlie the pathogenesis of ichthyosis in neutral lipid storage disease patients lacking functional CGI-58.

Fatty acids (FA)³ are major energy substrates and essential components of membrane lipids as well as of numerous bioac-

tive lipid species. Because excessive cellular concentrations of nonesterified FA are toxic, eukaryotic cells detoxify them by esterification to triacylglycerols (TG), which are subsequently stored in cellular lipid droplets (LD). Adipose tissue is the major storage organ for TG. However, some LD are found in essentially all cell types and tissues. Depending on the nutritional status and the energy demand of an organism, TG are synthesized (lipogenesis) or catabolized (lipolysis). Defects in the control of the finely regulated balance between lipogenesis and lipolysis result in the development of metabolic disorders such as obesity, type II diabetes, lipodystrophy, and neutral lipid storage disease (NLS) (1–6).

Hydrolysis of TG is mediated by the enzymatic activity of adipose triglyceride lipase (ATGL) (7–9) and hormone-sensitive lipase (10, 11). Whereas hormone-sensitive lipase-deficient mice exhibit a relatively benign phenotype (12, 13), mice lacking ATGL massively accumulate TG in multiple tissues, exhibit a severe defect in energy metabolism, and die prematurely due to cardiac dysfunction (14). Similarly, humans with mutations in the ATGL gene lacking normal enzyme function develop NLS associated with skeletal and cardiac myopathy (15). In severe cases, cardiomyopathy necessitates heart transplantation (16).

Studies in this laboratory and by others demonstrated that both human and murine ATGL are stimulated by a protein designated as CGI-58 (comparative gene identification-58) (17, 18) or ABHD5 (α/β -hydrolase domain containing-5) (19). Although the exact mechanism of the activation process is not understood, CGI-58 is known to be part of the lipolytic complex (20, 21). The protein binds to LD via interaction with proteins of the PAT family (*e.g.* perilipin, adipophilin, or muscle LD protein) (22). Hormonal stimulation leads to dissociation of CGI-58 from these binding partners and its translocation to the proximity of ATGL (23, 24). In addition to ATGL activation, CGI-58 was shown in *in vitro* experiments to acylate lysophosphatidic acid generating phosphatidic acid (25, 26). The physiological role of this reaction *in vivo* is currently unknown.

ease; ω -OH-ceramide, ω -hydroxyceramide; TG, triacylglycerol; BSA, bovine serum albumin; ES, embryonic stem; DMEM, Dulbecco's modified Eagle's medium; PBS, phosphate-buffered saline; NLS, neutral lipid storage disease with ichthyosis; UPLC, ultra performance liquid chromatography.

* This work was supported by Grant “GOLD-Genomics of Lipid-associated Disorders” (which is part of the Austrian Genome Project “GEN-AU Genome Research in Austria”) funded by the Austrian Ministry for Science and Research and by Grant SFB LIPOTOX F30-B05 and FWF Project P20602-B05 funded by the Austrian Fonds zur Förderung der Wissenschaftlichen Forschung.

[5] The on-line version of this article (available at <http://www.jbc.org>) contains supplemental Figs. S1 and S2.

¹ To whom correspondence may be addressed. Tel.: 43-316-380-1901; Fax: 43-316-380-9016; E-mail: rudolf.zechner@uni-graz.at.

² To whom correspondence may be addressed. Tel.: 43-316-380-1910; Fax: 43-316-380-9016; E-mail: guenter.haemmerle@uni-graz.at.

³ The abbreviations used are: FA, fatty acid; ATGL, adipose triglyceride lipase; CGI-58, comparative gene identification-58; CLE, cornified lipid envelope; DGAT2, acyl-CoA:diacylglycerol acyltransferase-2; MSMS, tandem mass spectrometry; LD, lipid droplet; LPAAT, lysophosphatidic acid acyltransferase; MEF, murine embryonic fibroblasts; NLS, neutral lipid storage dis-

The importance of CGI-58 for TG catabolism in humans is evident from clinical observations in patients affected with mutations in the gene encoding CGI-58. Mutant versions of CGI-58 fail to stimulate ATGL (17), and similarly to patients with ATGL mutations, individuals with defective CGI-58 accumulate TG in multiple tissues (15). However, the symptoms exhibited by the two groups of patients differ in two important ways. In contrast to patients with dysfunctional ATGL, CGI-58 mutations in humans are always associated with lamellar ichthyosis, a rare skin disorder, whereas myopathy, a hallmark of patients with NLSI associated with skeletal and cardiac myopathy, is less commonly observed. Accordingly, the disorder caused by defective CGI-58 was designated “neutral lipid storage disease with ichthyosis (NLSI)” (15), originally known as Chanarin-Dorfman syndrome (1, 2).

To address the potential rate-limiting role of CGI-58 in the regulation of cellular TG catabolism and to uncover currently unknown molecular mechanisms leading to disease development, we generated a CGI-58-deficient mouse model by disruption of exon 4–7 (coding for amino acids 172–351 of the mature protein), a gene region that has been linked to NLSI development in humans (17, 27). The observed phenotype of CGI-58-deficient mice included the following: (i) growth retardation, (ii) systemic TG accumulation in multiple tissues, and (iii) an impaired development of the skin permeability barrier.

EXPERIMENTAL PROCEDURES

Generation of CGI-58-deficient Animals—A 3.5-kb CGI-58 intron 3 sequence was amplified by PCR using HM-1 genomic embryonic stem (ES) cell DNA as template and cloned into pBlueKS(–) (Stratagene, La Jolla, CA) to generate the 5' part of the long arm of the targeting vector. The 3' part of the long arm of the targeting vector, a 6.0-kb genomic sequence encompassing CGI-58 exon 4–7, was amplified by PCR and cloned into pBlueKS(–). The 5' and 3' parts of the targeting vector were cloned upstream and downstream of a single loxP sequence flanked by compatible restriction sites. To generate the short arm, a 2.0-kb CGI-58 DNA fragment downstream to exon 7 was amplified and cloned into pBK-CMV harboring a loxP-flanked neomycin resistance cassette. Subsequently, the 3.2-kb DNA fragment encompassing the selection cassette and the short arm was cloned into the plasmid containing the long arm of the targeting vector. A diphtheria toxin A cassette was introduced 5' to the long arm to generate the final targeting vector. The linearized targeting vector was transfected into HM-1 ES cells by electroporation. G418-resistant clones were picked and expanded. Clones that underwent homologous recombination were transfected with a plasmid encoding Cre-recombinase (28) to generate ES cell clones harboring a null CGI-58 allele. Four independent clones were injected into 3.5-day-old C57Bl/6 blastocysts and transferred into pseudo-pregnant recipient mice. Chimeric animals with a high degree of coat color chimerism were bred with C57Bl/6 mice. Germ line transmission of the CGI-58 manipulated allele was observed by coat color and verified by Southern and Northern blotting. Genotyping of mice was routinely performed by PCR analysis of tail tip DNA using FIREPol® DNA polymerase (Solis BioDyne, Tartu, Estonia) and three primers in a single reaction as follows:

forward, 5'-GTC ATG GTT GTG GGG AAA TC-3'; reverse I, 5'-AGG AAG GGG TAT TCT GCA GG-3'; and reverse II, 5'-CTT CTT CCA GCT GCT TCT GC-3'. *Atgl*^{–/–} mice (ATGL knock-out mice) were generated as described previously (14). Animals were housed in a pathogen-free barrier facility (12-h light/dark cycle) and fed a standard laboratory chow.

Southern and Northern Blot Analysis—Genomic DNA was prepared with the DNeasy® blood and tissue kit (Qiagen Inc., Hilden, Germany) according to the manufacturer's protocol. For restriction fragment analysis, 10 µg of genomic DNA were digested with EcoRI restriction enzymes. DNA fragments were separated by agarose gel electrophoresis followed by depurination with 0.2 N HCl and denaturation with 0.5 N NaOH. After neutralization with Tris-HCl, pH 7.5, DNA was transferred onto a Hybond-N⁺ membrane (GE Healthcare) and hybridized with a ³²P-labeled probe. The external probe for DNA analysis was generated by PCR from HM-1 genomic ES cell DNA using the following primer pair: forward, 5'-GGA ATT CCC AGA CGC CAG TGA CTA AGG-3', and reverse, 5'-GGA ATT CAA CTC CTG CCT ATC TCT GTG G-3'. The PCR primers introduced the EcoRI restriction enzyme sites (underlined). The PCR product was ligated into the respective restriction enzyme site of pBlueKS(–) plasmid. For Northern blot analysis, total RNA was isolated from mouse tissue using the TRI Reagent® procedure according to the manufacturer's protocol (Invitrogen). Ten µg of total RNA were resolved by formaldehyde/agarose gel electrophoresis and blotted onto a Hybond-N⁺ membrane. Murine CGI-58 mRNA was hybridized with a ³²P-labeled murine CGI-58 cDNA probe generated by PCR from epididymal adipose tissue as described previously (17). Gene-specific probes for both Southern and Northern blot analysis were labeled with [α -³²P]dCTP (GE Healthcare) using the Prime-a-Gene® DNA labeling kit according to manufacturer's protocol (Promega, Madison, WI). After hybridization and washing, signals were visualized by exposure to PhosphorImager Screen (GE Healthcare).

Western Blot Analysis—15 µg of LD protein were separated by 10% SDS-PAGE according to standard protocols (29), blotted onto polyvinylidene fluoride membrane (Carl Roth GmbH, Karlsruhe, Germany), and hybridized with a rabbit polyclonal antiserum raised against murine CGI-58 (1:5,000 dilution; kindly provided by Dr. Dawn L. Brasaemle). Specifically bound immunoglobulins were detected in a second reaction using horseradish peroxidase-conjugated anti-rabbit IgG antibody (1:10,000 dilution) and visualized by enhanced chemiluminescence detection (ECL, GE Healthcare).

Murine Embryonic Fibroblast (MEF) Isolation and Experiments—MEF were derived from E12.5-day-old *Cgi-58*^{–/–} (CGI-58 knock-out mice), *Atgl*^{–/–}, and wild-type mouse embryos and cultured on gelatinized plates in Dulbecco's modified Eagle's medium (DMEM) containing 10% fetal bovine serum, 100 IU/ml penicillin (Invitrogen), and 100 µg/ml streptomycin. To investigate TG synthesis in MEF, confluent cell layers of MEF (passage 4) were incubated in the presence of oleic acid (200 and 400 µM, respectively) bound to defatted BSA at a molar FA/BSA ratio of 3:1. After 24 h, the medium was removed; cells were washed twice with PBS, and the cellular TG

CGI-58 Deficit Impairs Hepatic and Epidermal TG Catabolism

content was measured as outlined below. For *in vivo* radiolabeling of MEF TG stores, confluent cell layers were incubated for 24 h with 400 μM oleate (containing 2.5 μCi of [9,10- ^3H]oleic acid/ μmol of oleate) bound to BSA at a molar FA/BSA ratio of 3:1. LD were isolated and purified by density gradient centrifugation as described previously (17). For determining LD TG and protein concentrations, aliquots of LD preparations were adjusted to a final concentration of 0.1% (v/v) Triton X-100. TG and protein concentrations were measured using commercial kits (Thermotrace triglycerides reagent, Thermo Electron Corp., Victoria, Australia, and Bradford protein assay, Bio-Rad) and were found to be comparable in all preparations (typically 80 μg of protein/ μmol of TG). The LD TG hydrolase activities were determined by self-digestion of purified LD as described previously (17).

Assay for Skin and Liver TG Hydrolase Activity—Full thickness skin and liver were surgically prepared; subcutaneous tissue was scraped off, and skin and liver tissue were washed in ice-cold PBS supplemented with 100 units/ml heparin and 1 mM EDTA. Epidermis was separated from dermis by incubating skin tissue in PBS containing 10 mM EDTA and 1 g/liter glucose at 37 °C for 45 min. Homogenization of tissues was performed on ice in buffer A (0.25 M sucrose, 1 mM EDTA, 1 mM dithiothreitol, 20 $\mu\text{g}/\text{ml}$ leupeptin, 2 $\mu\text{g}/\text{ml}$ antipain, 1 $\mu\text{g}/\text{ml}$ pepstatin, pH 7.0) using an Ultra Turax (IKAR, Janke & Kunkel, Germany). After centrifugation at 20,000 $\times g$ and 4 °C for 30 min, the infranatant was subjected to ultracentrifugation at 100,000 $\times g$ and 4 °C for 90 min. The TG-free infranatant was assayed using a phospholipid-emulsified triolein (330 μM) substrate containing [9,10- ^3H]triolein (PerkinElmer Life Sciences) with or without addition of 200 ng of GST-tagged CGI-58 (GST-CGI-58) as described previously (17).

Lipid Analysis—Total lipids were extracted twice from murine total carcass or tissue homogenates with chloroform/methanol/glacial acetic acid (66:33:1, v/v), and phase separation was achieved by the addition of water. Total lipids from MEF were extracted three times in hexane/isopropyl alcohol (3:2, v/v). After lipid extraction, tissue homogenates or MEF were solubilized in 0.3 N NaOH, 0.1% (w/v) SDS at 65 °C for several hours, and the protein content was determined using BCA reagent (Pierce) and BSA as standard. For the extraction of covalently bound lipids, the alkaline-hydrolyzed samples were extracted with chloroform/methanol/glacial acetic acid (66:33:1, v/v). After centrifugation (1,400 $\times g$, 15 min), the lower organic phase was collected, and lipids were analyzed as described below.

Lipids were dried, reconstituted in chloroform, and spotted onto a Silica Gel 60 plate (Merck). Neutral lipids were resolved in hexane/diethyl ether/glacial acetic acid (70:29:1, v/v) with authentic standards. Epidermal ceramide species were separated twice using chloroform/methanol/glacial acetic acid (190:9:1 v/v/v) as solvent system (30). Spots were visualized by established carbonization method or with iodine vapor, and radioactivity was measured by liquid scintillation counting. Dried lipids of murine tissues or MEF were redissolved in 1% (v/v) Triton X-100, and TG content was measured using Infinity triglycerides reagent (Thermo Electron Corp., Victoria, Australia).

ω -Hydroxyceramides (ω -OH-ceramides), acylceramides, and phospholipids were analyzed by tandem mass spectrometry (MSMS) using a Quantum TSQ (Thermo), coupled to an Accela ultra performance liquid chromatography (UPLC) system (Thermo). The column was a Thermo Hypersil GOLD, 100 \times 1 mm (1.9 μm), and operated at 50 °C. Water (solvent A) and acetonitrile/isopropyl alcohol (5:2, v/v, solvent B), both containing 1% of NH_4Ac (1 M aqueous solution) and 0.1% formic acid, were used as solvent system. The gradient started with 35% solvent B, increased to 70% within 4 min, then to 100% within 16.5 min, and remained at 100% for 9.5 min. After the analysis, the column was equilibrated at starting conditions for 5 min. The flow rate was 0.250 ml/min. Ionization was performed by a heated electrospray ionization operating in the positive ion mode with a spray voltage of 4,000 V. Ceramide species were identified by a precursor ion scan for the characteristic fragment at m/z 264.3. Argon was used as collision gas. The collision energy was set to 30 V for analyses of ω -OH-ceramides and to 50 V for acylceramides. Collision gas pressure was 0.7 millitorr. Samples were diluted with solvent B, and *N*-(dodecanoyl) sphing-4-enine (Avanti Polar Lipids Inc., Alabaster, AL) was added as an internal standard. Phosphatidylcholine species were measured by a precursor ion scan for the characteristic fragment at m/z 184.1 and 30 V collision energy. Phosphatidylethanolamine species were measured by a neutral loss scan for m/z 141.0 and 25 V collision energy. Phosphatidylcholine and phosphatidylethanolamine 24:0 (12:0/12:0, Avanti Polar Lipids Inc.) were added as internal standard, respectively.

Labeling of Epidermal Lipids—Radiolabeling of lipid species in the epidermis was performed as described for cultured skin fibroblasts (31). In brief, dorsal 3 \times 3-mm sized epidermal sheets were incubated in DMEM containing 1% (w/v) delipidated BSA and 400 μM oleate (12.5 $\mu\text{Ci}/\mu\text{mol}$ oleate) bound to delipidated BSA at a molar FA/BSA ratio of 3:1. After 5 h, epidermal sheets were washed with PBS and chased in the presence or absence of 20 μM orlistat in DMEM containing 1% (w/v) delipidated BSA. At various time points, epidermal sheets were washed, and lipids were extracted with chloroform/methanol/glacial acetic acid (66:33:1, v/v), separated by TLC, and measured as described above.

Blood Chemistry—Anesthetized newborn mice were sacrificed by decapitation. Blood samples were collected using a Microvette[®] CB 300 (Sarstedt, Nümbrecht, Germany). Plasma FA and TG concentrations were determined using commercial kits (Wako Chemicals, Neuss, Germany; Thermo Electron Corp., Victoria, Australia). Blood glucose levels were measured using blood glucose strips and the Accu-Check glucometer (Roche Diagnostics).

Histology, Immunohistochemistry, and Electron Microscopy—Skin pieces were fixed overnight in 4% neutral buffered formalin and embedded in paraffin, cut into 4–6- μm -thick sections, and stained with hematoxylin and eosin using established protocols. For visualization of vacuoles within granulocytes, blood smears from newborn mice were stained by combined May-Grünwald-Giemsa according to established protocols. To visualize neutral lipids in liver tissue, tissue samples were snap-frozen in liquid nitrogen, sectioned, and stained with Sudan III

following a standard protocol. For determination of keratinocyte differentiation and proliferation, antibodies against cytokeratin 14 (CK14, Novocastra Laboratories, Newcastle upon Tyne, UK), cytokeratin 6 (CK6, Covance Inc., Emeryville, CA), fillagrin (Fila, Covance), and Ki67 (Novocastra) were evaluated for use on formaldehyde-fixed paraffin-embedded tissue specimens using different methods of pretreatment. Tissue sections were deparaffinized by xylene, rehydrated in graded alcohols, and submitted to microwave epitope retrieval (40 min at 150 watts in 0.01 M sodium citrate buffer, pH 6.0). After treatment in 1% H₂O₂ for 10 min, sections were incubated for 1 h using Dako antibody-diluent (Dako, Vienna, Austria). Final dilutions were as follows: cytokeratin 14 (1:50), cytokeratin 6 (1:500), fillagrin (1:500), and Ki67 (1:500). After enhancement using MultiLink Dako (E0453) diluted 1:100 and StreptABComplex/horseradish peroxidase Dako (K0377) diluted 1:100 for 30 min each, detection was performed using AEC Substrate Chromogen Ready-to-Use (Dako K3464) under microscopic control. For electron microscopy, tissue was fixed in 2.5% glutaraldehyde in 0.01 M cacodylate buffer, pH 7.3, dehydrated, and embedded in resin (AGAR-100, Agar Scientific, Essex, UK). 50-nm-thick sections were contrasted with uranyl acetate/lead citrate and studied in a Philips CM 100 electron microscope.

Skin Permeation Assay and Skin Grafts—Newborn mice were euthanized, immersed in PBS containing 0.1% toluidine blue (Sigma) for 4 h, and photographed (32). Full-thickness skin pieces (~1 cm²) from newborn wild-type and *Cgi-58*^{-/-} mice were grafted onto the left and right sides of athymic nude mice (Charles River Laboratories, Sulzfeld, Germany). Wound edges were sutured. After 3 weeks, the grafted skin was investigated for hair growth, and sections were stained for differentiation markers as described above.

Statistical Analysis—Statistical significance was determined by the Student's unpaired *t* test (two-tailed). Group differences considered significant for *p* < 0.05 (*), *p* < 0.01 (**), and *p* < 0.001 (***)

RESULTS

Generation of CGI-58-deficient Mice—To investigate the physiological role of CGI-58 *in vivo*, we generated mice lacking functional CGI-58. For that purpose, we designed a targeting vector harboring a loxP-flanked neomycin resistance gene cassette (*neo*) downstream to the polyadenylation sequence and an additional loxP recombination site in intron 3 of the murine *cgi-58* gene (Fig. 1A). This vector was electroporated into ES cells. Cells that underwent homologous recombination were selected and subsequently transfected with a plasmid encoding Cre-recombinase. ES cell clones harboring a CGI-58 null allele were used for blastocyst injection to generate CGI-58-deficient mice. Southern blot analysis of mouse genomic DNA confirmed the disruption of the *Cgi-58* gene (Fig. 1B). *Cgi-58*^{-/-} mice showed no expression of CGI-58 mRNA analyzed by Northern blotting (Fig. 1C). Mice heterozygous for the targeted allele exhibited ~50% reduced CGI-58 mRNA expression levels compared with wild-type mice. CGI-58 protein levels in *Cgi-58*^{-/-} mice were analyzed by Western blot analysis of LD proteins isolated from newborn mice (Fig. 1D). Using a polyclonal

rabbit anti-CGI-58 antiserum, wild-type and heterozygous *Cgi-58*^{+/-} mice exhibited a signal specific for CGI-58 protein at the expected molecular mass of 39 kDa, which was not detectable in *Cgi-58*^{-/-} mice.

Growth Retardation, Postnatal Death, and NLSI with Ichthyosis in Mice Lacking CGI-58—*Cgi-58*^{-/-} mice died within 16 h after birth, were smaller, and weighed less than wild-type littermates (Fig. 2A and Table 1). Genotype analysis of 1042 newborn animals from 143 heterozygous intercrosses demonstrated normal Mendelian distribution of the mutant CGI-58 allele (wild-type 253, 24.3%; heterozygous 535, 51.3%; *Cgi-58*^{-/-} 254, 24.4%; *p* < 0.001 by χ^2 test). The lack of CGI-58 was associated with ectopic lipid accumulation as evident from increased TG content in carcasses (1.8-fold, Fig. 2B) and granulocyte vacuolization (Jordans' anomaly) (Fig. 2C) (33). Histological analysis of *Cgi-58*^{-/-} epidermis exhibited hyperkeratosis characterized by tightly condensed lamellar sheets in the stratum corneum and increased numbers of cell layers in the stratum spinosum (Fig. 2D). These alterations are characteristics for lamellar ichthyosis and indicate that mice with defective CGI-58 develop a condition similar to human NLSI.

Circulating energy substrates were markedly decreased in *Cgi-58*^{-/-} mice (Table 2). Although plasma concentrations of FA, TG, and glucose in heterozygous *Cgi-58*^{+/-} mice were comparable with those in wild-type mice, they were decreased by 60, 48, and 74% in *Cgi-58*^{-/-} mice, respectively. Considering that the marked hypoglycemia may cause the early death of *Cgi-58*^{-/-} mice, glucose was injected to transiently raise plasma glucose levels. However, this treatment did not rescue *Cgi-58*^{-/-} mice from premature death. Similarly, increasing humidity and application of Vaseline® to the skin of newborns to prevent desiccation of the animals failed to significantly prolong the life span of *Cgi-58*^{-/-} mice.

CGI-58 Is Rate-limiting in MEF TG Catabolism via Activation of ATGL Enzyme Activity—To define the impact of CGI-58 deficiency on cellular TG metabolism, we isolated MEF from E12.5-day-old *Cgi-58*^{-/-}, *Atgl*^{-/-}, and wild-type embryos and incubated these cells with increasing concentrations of oleic acid to induce lipogenesis. TG accumulation was increased in both *Cgi-58*^{-/-} and *Atgl*^{-/-} MEF (1.6- and 1.9-fold, respectively, at 400 μ M oleic acid) compared with wild-type MEF (Fig. 3A). Concomitantly, the LD-associated TG hydrolase activities of *Cgi-58*^{-/-} and *Atgl*^{-/-} MEF were decreased by 76 and 81%, respectively, compared with wild-type MEF (Fig. 3B). Defective lipolysis was partially rescued by addition of purified, recombinant GST-CGI-58 to LD of *Cgi-58*^{-/-} MEF (Fig. 3B) but not of *Atgl*^{-/-} MEF. Taken together, these findings suggest that excessive lipid storage in *Cgi-58*^{-/-} MEF is caused by defective activation of ATGL-mediated TG hydrolysis.

Hepatic Steatosis in *Cgi-58*^{-/-} Mice Is Associated with Impaired TG Catabolism—To address the role of CGI-58 in liver TG catabolism, we measured TG concentrations and TG hydrolase activities in liver lysates from newborn *Cgi-58*^{-/-}, *Atgl*^{-/-}, and wild-type mice. Liver TG contents (Fig. 4A) were markedly increased in *Cgi-58*^{-/-} (4.1-fold) and *Atgl*^{-/-} mice (4.6-fold) compared with wild-type newborns. Sudan III staining of histological liver sections from

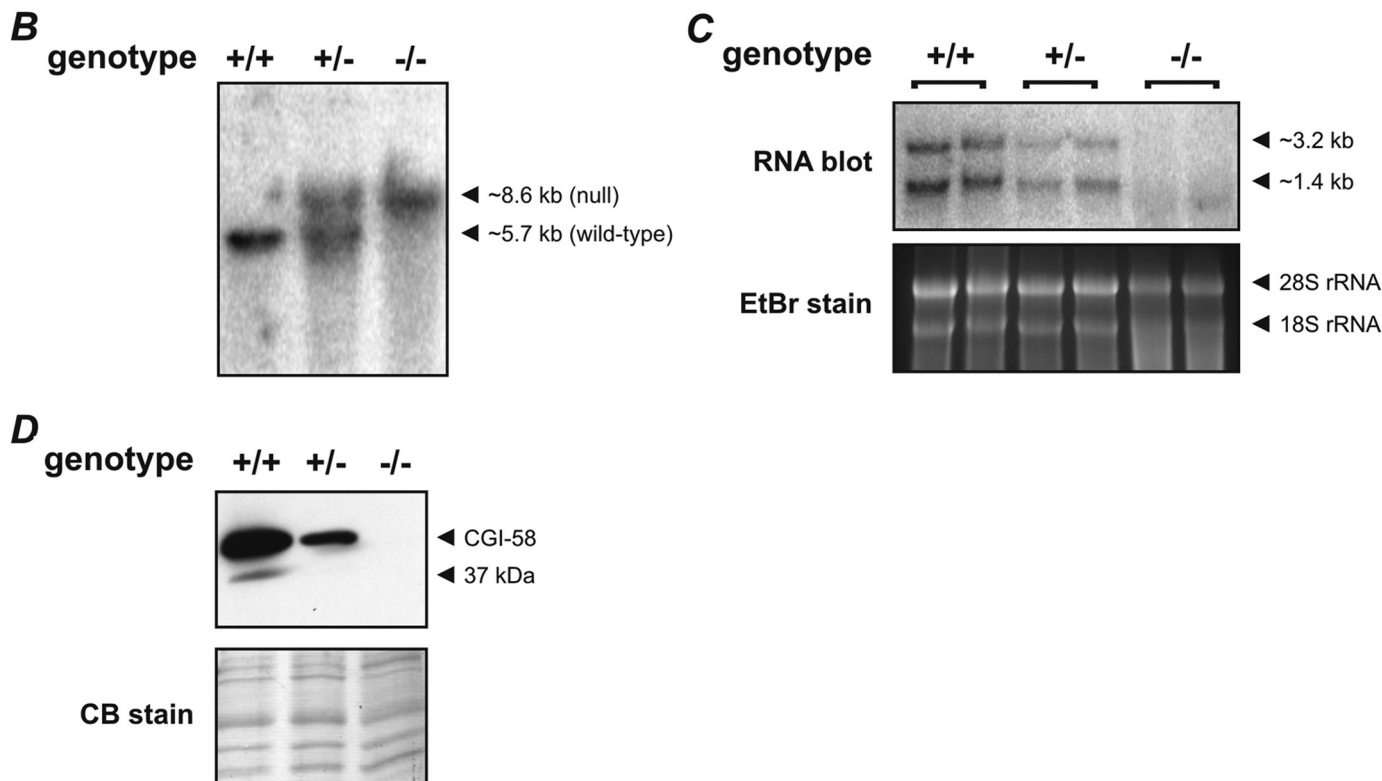
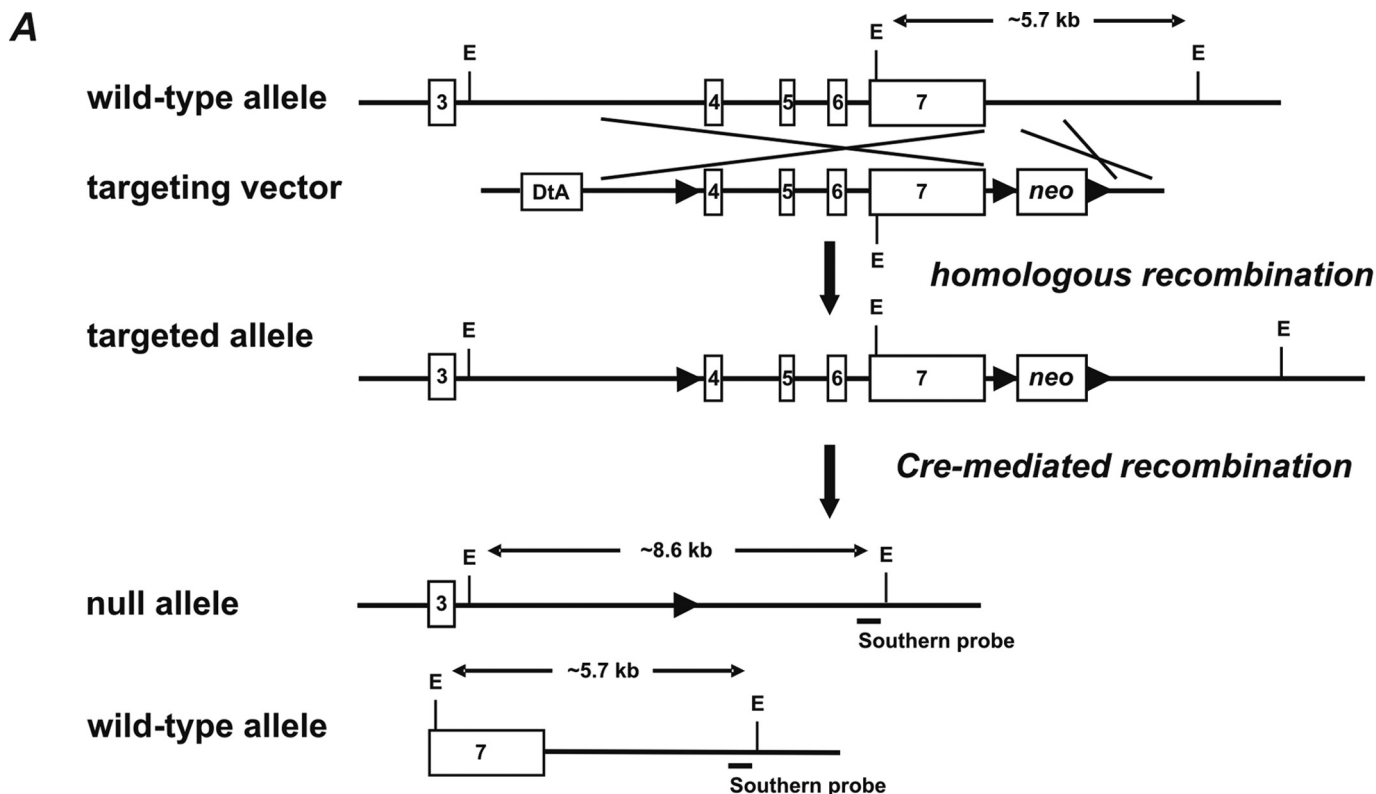
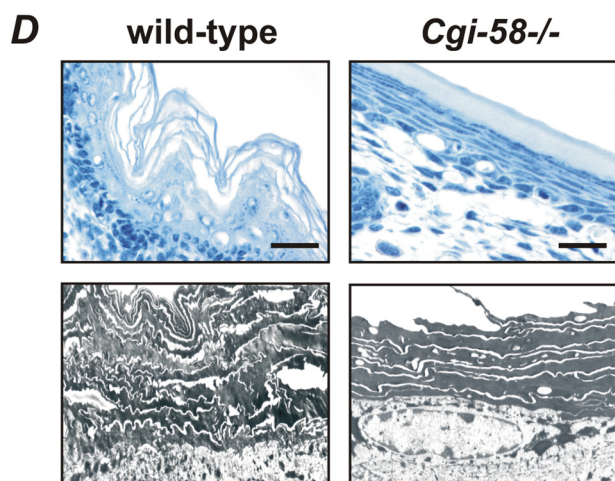
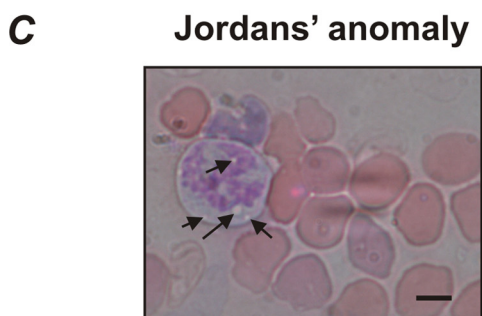
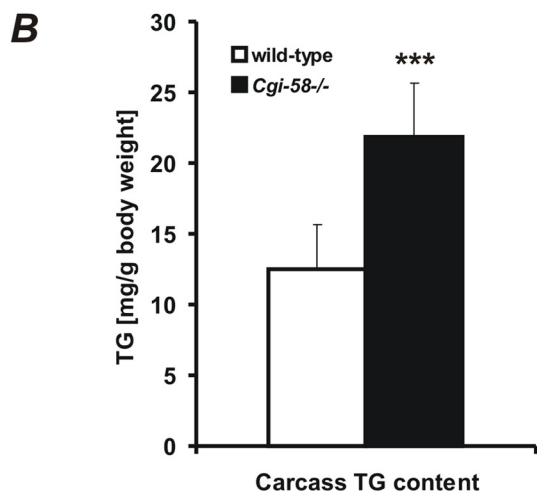
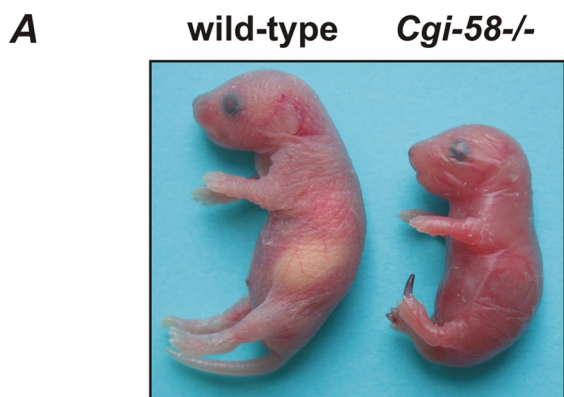


FIGURE 1. Targeting strategy and generation of CGI-58-deficient mice. *A*, homologous recombination of the targeting vector with the wild-type allele resulted in the introduction of a loxP site (▶) into intron 3 and a neomycin resistance gene cassette flanked by loxP sites into the downstream sequence of exon 7. Subsequent Cre-recombinase-mediated recombination among the distal loxP sites resulted in the deletion of exons 4–7. The targeted allele was identified by EcoRI (*E*) restriction digest and hybridization with an external Southern probe (solid bar) revealing an 8.6-kb DNA fragment. *B*, DNA from newborn mice was restriction-digested with EcoRI and analyzed by Southern blotting using an external probe specific for the downstream region of the *Cgi-58* gene. Autoradiography signals obtained from DNA fragments of 5.7 and 8.6 kb corresponded to wild-type (+) and targeted CGI-58 (–) alleles, respectively. *C*, Northern blotting analysis of CGI-58 mRNA expression levels was performed with total carcass RNA using a probe specific for the coding sequence of CGI-58. RNA gel was stained with ethidium bromide (*EtBr*) as loading control. *D*, Western blotting analysis of CGI-58 protein expression levels was performed with proteins of carcass lipid droplets using a rabbit polyclonal CGI-58 antiserum. Polyvinylidene fluoride membrane was stained with Coomassie blue (*CB*) as loading control.

**TABLE 1**

Comparison of size and weight of newborn wild-type, *Cgi-58*^{+/-}, and *Cgi-58*^{-/-} mice

Data are means ± S.D. (*n* = 14). Statistical significance was determined by the two-tailed Student's *t* test.

	Wild type	<i>Cgi-58</i> ^{+/-}	<i>Cgi-58</i> ^{-/-}
Length (mm)	30.4 ± 0.63	30.2 ± 0.75	25.6 ± 0.65 ^a
Weight (g)	1.36 ± 0.090	1.36 ± 0.102	1.09 ± 0.088 ^a

^a Statistical significance was determined by the two-tailed Student's *t*-test, *p* < 0.001.

TABLE 2

Comparison of blood parameters in newborn wild-type, *Cgi-58*^{+/-}, and *Cgi-58*^{-/-} mice

All parameters were measured 10–14 h postpartum. Data are means ± S.D. (*n* = 5–6).

	Wild type	<i>Cgi-58</i> ^{+/-}	<i>Cgi-58</i> ^{-/-}
FA (mmol/liter)	0.50 ± 0.076	0.46 ± 0.104	0.20 ± 0.038 ^a
TG (mg/deciliter)	69.7 ± 11.31	60.0 ± 14.18	36.2 ± 8.87 ^b
Glucose (mg/deciliter)	67 ± 8.2	61 ± 6.6	16 ± 5.6 ^a

^a Statistical significance was determined by the two-tailed Student's *t* test, *p* < 0.01.

^b Statistical significance was determined by the two-tailed Student's *t* test, *p* < 0.001.

Cgi-58^{-/-} and *Atgl*^{-/-} newborns confirmed an increase of neutral lipid content (Fig. 4B). In parallel, liver TG hydrolase activities (Fig. 3C) were significantly decreased in *Cgi-58*^{-/-} (–73%) and *Atgl*^{-/-} mice (–46%). The addition of recombinant GST-CGI-58 (Fig. 4C) substantially stimulated TG hydrolysis (8.6-fold) in CGI-58-deficient liver lysates and exceeded wild-type TG hydrolase activities (1.7-fold). In contrast, addition of recombinant GST-CGI-58 to ATGL-deficient liver lysates caused a marginal increase in TG hydrolase activities (1.2-fold).

Defective Skin Permeability Barrier and Keratinocyte Differentiation of CGI-58-deficient Skin—To assess whether the distinct morphological alterations particularly in the stratum corneum of the *Cgi-58*^{-/-} epidermis (Fig. 2D) are associated with a loss of the skin permeability barrier function, we investigated the penetration of an aqueous toluidine blue solution into the epidermis of newborn mice. *Cgi-58*^{-/-} mice showed massive staining when exposed to toluidine blue for 4 h indicating a leaky skin barrier (Fig. 5A). Wild-type or *Atgl*^{-/-} pups were completely resistant to toluidine blue permeation consistent with an intact skin barrier function.

Immunohistochemical analysis of the epidermis revealed delayed keratinocyte differentiation in *Cgi-58*^{-/-} compared with wild-type mice (Fig. 5B). In the healthy skin, cytokeratin 14, a marker of proliferating basal keratinocytes, was almost exclusively present in basal cells of the squamous epithelium.

FIGURE 2. Murine CGI-58 deficiency causes NLSD with ichthyosis. A, photograph of newborn wild-type and *Cgi-58*^{-/-} mice. Note the glossy dry skin, the smaller size of the body, and necrotic tail tip. B, carcasses of newborn wild-type, *Cgi-58*^{-/-}, and *Atgl*^{-/-} mice were homogenized, and lipids were extracted. The TG content was determined enzymatically and normalized to body weight. Data are means ± S.D. (*n* = 4–6). Statistical significance was determined by the two-tailed Student's *t* test (***, *p* < 0.001). C, peripheral blood smear of *Cgi-58*^{-/-} newborn was stained with May-Grünwald-Giemsa. Arrows indicate granulocyte vacuolization (Jordans' anomaly). D, skin sections of newborn wild-type and *Cgi-58*^{-/-} mice were stained with hematoxylin/eosin for light microscopy (upper panel, scale bars represent 20 μm) or contrasted with uranyl acetate/lead citrate for transmission electron microscopy at ×5,000 magnification (lower panel).

CGI-58 Deficit Impairs Hepatic and Epidermal TG Catabolism

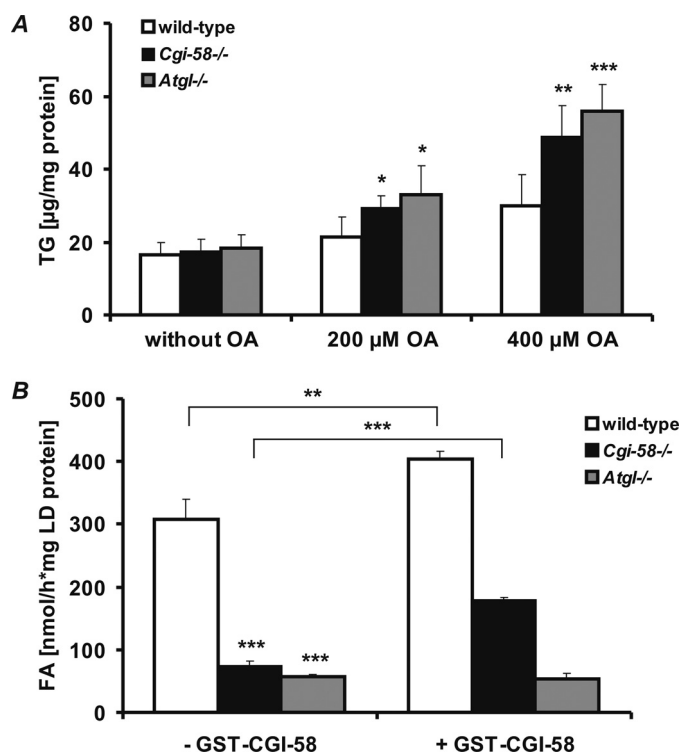


FIGURE 3. MEF lacking CGI-58 and ATGL accumulate TG and exhibit reduced TG hydrolase activity. A and B, wild-type, *Cgi-58*^{-/-}, and *Atgl*^{-/-} MEF were incubated in the absence or presence of oleic acid (OA, 200 and 400 μ M, respectively) to promote cellular TG accumulation (A) or with [9,10-³H]oleate for determination of LD-associated TG hydrolase activity (B). After 24 h, cellular TG content was determined enzymatically (A) or radiolabeled LD were purified by gradient ultracentrifugation, and TG hydrolase activity was determined by self-digestion in the absence or presence of recombinant purified GST-CGI-58 as described previously (17) (B). Data are means \pm S.D. and representative for three independent experiments. Statistical significance was determined by the two-tailed Student's *t* test (*, $p < 0.05$; **, $p < 0.01$; ***, $p < 0.001$).

In *Cgi-58*^{-/-} skin sections, cytokeratin 14 staining was much more diffuse reaching into upper layers of the stratum spinosum. Cytokeratin 6 is usually expressed in the outer root sheath of hair follicles and nail beds and not detected in the interfollicular epidermis. Increased cytokeratin 6 expression is typically observed in hyper-proliferating epithelia or aberrant epidermal differentiation as seen in ichthyosis and psoriasis (34). Consistent with this defect, pronounced cytokeratin 6 protein was observed in the epidermis of *Cgi-58*^{-/-} but not in wild-type skin. Fillagrin, a marker for terminally differentiated keratinocytes, was barely detectable in *Cgi-58*^{-/-} sections but clearly visible in wild-type skin samples. Notably, the localization of the cell proliferation marker Ki67 (35) was not changed in *Cgi-58*^{-/-} compared with wild-type epidermis (Fig. 5B, lowest panel). Taken together, the immunohistochemical analysis revealed that CGI-58 deficiency results in delayed keratinocyte differentiation and corneocyte formation, which may contribute to the dysfunctional stratum corneum.

To investigate whether the skin defect is specifically caused by the lack of CGI-58 in the skin and not by a defect of the metabolite supply from the circulation, we transplanted *Cgi-58*^{-/-} skin grafts onto nude mice. As shown in Fig. 6A, *Cgi-58*^{-/-} transplants exhibited severe growth retardation

and lacked fur development on the recipient organism. In comparison, control grafts derived from wild-type newborns developed normally on nude mice. Thus, the lack of CGI-58 in the transplanted skin cannot be compensated by physiological CGI-58 expression and function in tissues of the recipient organism. As shown in the skin sections of newborn *Cgi-58*^{-/-} mice, cytokeratin 14 staining, typically observed in the basal layer of the epidermis, and cytokeratin 6 staining were present in an extended area of *Cgi-58*^{-/-} skin grafts (Fig. 6B). Apparently, defective skin development due to the absence of CGI-58 reflects a direct requirement for the protein in the skin and is not caused by systemic CGI-58 deficiency.

Impaired Skin TG Catabolism Affects Generation of Essential Epidermal Lipids in the Cgi-58^{-/-} Epidermis—Epidermal differentiation is known to involve remodeling of lipid stores and synthesis of certain lipid classes such as acylceramides, wax esters, and phospholipids. Because CGI-58 plays a central role in TG catabolism of several tissues and cell types, we hypothesized that inadequate generation of TG metabolites in CGI-58-deficient skin could impact keratinocyte differentiation and permeability barrier function. Therefore, we determined the TG content in the skin of newborn *Cgi-58*^{-/-}, *Atgl*^{-/-}, and wild-type mice. Both dermal and epidermal TG contents were significantly increased in *Cgi-58*^{-/-} (1.5- and 2.0-fold, respectively) and *Atgl*^{-/-} (1.6- and 1.3-fold, respectively) compared with wild-type skin (Fig. 7A). Consistent with the elevated dermal TG levels, TG hydrolase activities were markedly decreased in dermal lysates of both *Cgi-58*^{-/-} (-51%) and *Atgl*^{-/-} (-52%) mice compared with those of wild-type mice (Fig. 7B). Notably, although epidermal TG hydrolase activities were drastically decreased in lysates of *Cgi-58*^{-/-} animals (-81%), they were completely unaffected in lysates of *Atgl*^{-/-} mice. Addition of recombinant GST-CGI-58 significantly improved both epidermal and dermal TG hydrolase activities in lysates of *Cgi-58*^{-/-} mice but did not affect TG hydrolysis of *Atgl*^{-/-} samples (data not shown). These findings are in line with the concept that in wild-type epidermis a “non-ATGL” TG hydrolase is active in a manner that depends on CGI-58 stimulation.

Acylceramides are obligatory precursors for the covalent binding of ω -OH-ceramides to corneocyte proteins (predominantly involucrin) and the formation of a water-resistant structure in the stratum corneum, also designated as cornified lipid envelope (CLE) (36). To investigate whether the skin barrier defect in *Cgi-58*^{-/-} mice is linked to changes in epidermal ceramide metabolism, we measured the concentrations of ω -OH-ceramides covalently bound to the CLE, free extractable, unbound ω -OH-ceramides, and acylceramides in the epidermis of newborn *Cgi-58*^{-/-}, *Atgl*^{-/-}, and wild-type mice by UPLC-MS/MS. All species of covalently bound ω -OH-ceramides were drastically decreased (supplemental Fig. S1A) in *Cgi-58*^{-/-} epidermis. The total of covalently bound ω -OH-ceramides (as calculated from the sum of individual covalently bound ω -OH-ceramide species) was decreased by 85 and 84% in *Cgi-58*^{-/-} epidermis compared with wild-type and *Atgl*^{-/-} epidermis, respectively (Fig. 8A). In contrast, free ω -OH-ceramide species, which were barely detectable in wild-type and *Atgl*^{-/-} mice, were substantially increased in *Cgi-58*^{-/-} samples

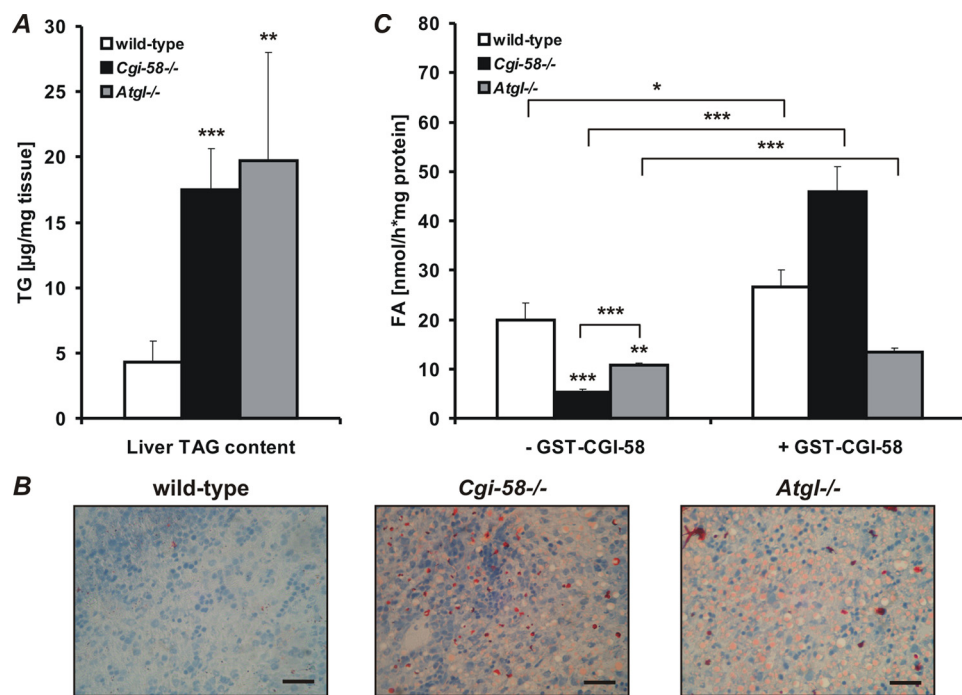


FIGURE 4. TG accumulation and defective TG catabolism in CGI-58-deficient mice. *A*, livers of newborn wild-type, *Cgi-58*^{-/-}, and *Atgl*^{-/-} mice were homogenized, and lipids were extracted. The TG content was determined enzymatically and normalized to tissue weight. Data are means \pm S.D. ($n = 5$). *B*, liver sections of newborn wild-type, *Cgi-58*^{-/-}, and *Atgl*^{-/-} mice were stained with Sudan III/hematoxylin and analyzed by light microscopy. Scale bars represent 50 μ m. *C*, TG hydrolase activities of liver lysates from newborn wild-type, *Cgi-58*^{-/-}, and *Atgl*^{-/-} mice were determined in the absence or presence of recombinant purified GST-CGI-58 using phospholipid-emulsified triolein substrate, containing [9,10-³H]triolein as tracer. Release of radiolabeled FA was determined by liquid scintillation counting. Data are means \pm S.D. ($n = 5$) and representative for three independent experiments. Statistical significance was determined by the two-tailed Student's *t* test (*, $p < 0.05$; **, $p < 0.01$; ***, $p < 0.001$).

(supplemental Fig. S1B). The total of free ω -OH-ceramide species was 13.5-fold higher in *Cgi-58*^{-/-} epidermis compared with wild-type samples and 9.3-fold higher compared with *Atgl*^{-/-} samples (Fig. 8A). Strikingly, acylceramides were undetectable in the *Cgi-58*^{-/-} epidermis (Fig. 8A and supplemental Fig. S1C).

Acylceramides are generated by esterification of free ω -OH-ceramides with primarily oleic or linoleic acid (36). Whether oleic or linoleic acid originates from the cellular nonesterified FA or the LD TG pool is currently unknown. We hypothesized that the impaired TG hydrolase activity and consequently the decreased release of oleic acid from the TG pool in *Cgi-58*^{-/-} epidermis may prevent acylceramide formation. To test this hypothesis, we analyzed the incorporation of exogenously added oleic acid into acylceramides of epidermal sheets derived from newborn *Cgi-58*^{-/-} and wild-type mice *in vitro*. After 5 h of pulse labeling with 400 μ M oleate (including [9,10-³H]oleate as tracer), epidermal sheets were chased for a period of 6 h, and radioactivity in the TG, phospholipid (phosphatidylcholine and phosphatidylethanolamine), and acylceramide fractions was measured (Fig. 8, B–D). Under these conditions, the radioactivity in the TG pool of wild-type epidermal cultures declined (Fig. 8B), whereas it increased in both the phospholipid (Fig. 8C) and acylceramide fractions (Fig. 8D) over time. In contrast, in *Cgi-58*^{-/-} epidermis the radioactivity remained in the TG pool, consistent with the concept that oleic acid is not released from TG and becomes trapped within LD. Accordingly, the transfer of labeled oleic acid to

phospholipids and more importantly to acylceramides was attenuated in *Cgi-58*^{-/-} epidermis (Fig. 8, C and D). To analyze whether the sequestration of FA in TG affects the epidermal phospholipid species, we determined amounts and FA composition of major phospholipids (phosphatidylcholine and phosphatidylethanolamine) by UPLC-MSMS in extracts of *Cgi-58*^{-/-}, *Atgl*^{-/-}, and wild-type mice (supplemental Fig. S2, A and B). In contrast to ω -OH-ceramides and acylceramides, phosphatidylcholine and phosphatidylethanolamine species were unchanged in the epidermis of *Cgi-58*^{-/-} as compared with wild-type and *Atgl*^{-/-} mice.

To confirm the crucial role of epidermal TG catabolism for acylceramide synthesis, we measured the transfer of oleic acid from TG to acylceramides of wild-type tissue cultures in the absence or presence of orlistat, a potent lipase inhibitor impairing TG hydrolysis (Fig. 8, E–G) (37). Similarly as observed in *Cgi-58*^{-/-} epidermis, the TG catabolism was impaired in the presence

of orlistat, and no transfer of radioactivity from TG to phospholipids and acylceramides was observed (Fig. 8, F and G). In contrast, in the absence of orlistat the radioactivity in the TG fraction decreased, whereas the incorporation of radioactivity into phospholipids and acylceramides increased (Fig. 8, F and G). As orlistat shows little or no effect on phospholipase activities (37), these findings further demonstrate the essential role of epidermal TG catabolism for acylceramide synthesis and the development of an intact skin permeability barrier.

DISCUSSION

To elucidate the physiological function of CGI-58 in lipid homeostasis and skin development, we generated and characterized a CGI-58 knock-out mouse model. We show that *Cgi-58*^{-/-} mice exhibit growth retardation, systemic TG accumulation in multiple tissues, and hepatic steatosis. They display severely reduced plasma TG, FA, and glucose levels. Notably, the animals suffer from impaired development of the skin permeability barrier resulting in rapid dehydration. Because newborn mice virtually exhibit no white adipose tissue, they are dependent on suckling maternal milk. However, *Cgi-58*^{-/-} mice did not suckle. The severe skin phenotype combined with profound alterations in energy supply leads to the early death of *Cgi-58*^{-/-} animals within 1 day after birth.

CGI-58 was previously shown to markedly increase TG hydrolase activity of ATGL (17). Consistent with these

CGI-58 Deficit Impairs Hepatic and Epidermal TG Catabolism

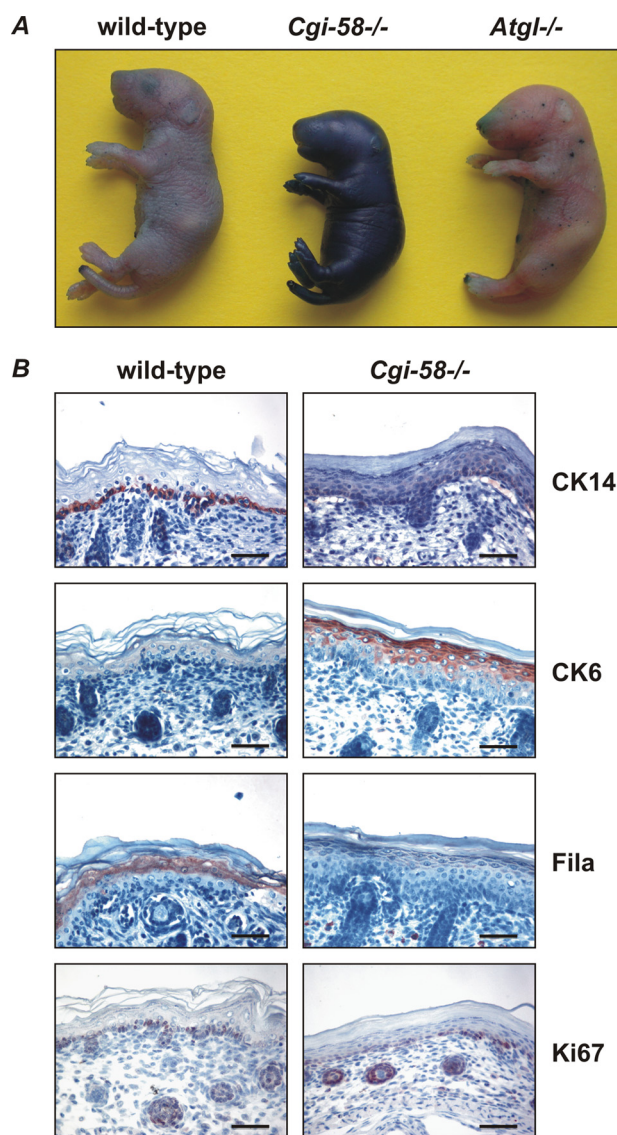


FIGURE 5. CGI-58 deficiency disrupts the epidermal permeability barrier and affects keratinocyte differentiation. A, euthanized newborn wild-type, *Cgi-58*^{-/-}, and *Atgl*^{-/-} mice were immersed for 4 h in toluidine blue dye solution, rinsed with PBS, and photographed. B, skin sections of newborn wild-type and *Cgi-58*^{-/-} mice were stained with antibodies specific for cytokeratin 14 (CK14), cytokeratin 6 (CK6), filaggrin (*Fila*), or Ki67 and analyzed by light microscopy. Scale bars represent 50 μ m.

in vitro observations, *Cgi-58*^{-/-} mice exhibited increased TG contents in the whole carcass, the liver, and cultured MEF. The magnitude of lipid accumulation in newborn CGI-58-deficient animals or cultivated cells was similar to that observed in ATGL-deficient mice. Comparative analysis of TG storage and LD-associated TG hydrolase activities in *Cgi-58*^{-/-} and *Atgl*^{-/-} MEF revealed that a defect in ATGL activation accounts for excessive neutral lipid storage. Accordingly, CGI-58 exhibits a crucial role in cellular TG homeostasis and energy catabolism via its impact on regulating ATGL activity. Unfortunately, the lethal phenotype within hours after birth prevented an extensive characterization of the metabolic consequences of systemic lipid accumulation, such as energy substrate utilization or insulin response. Elucidation of the tissue-specific effects of CGI-58

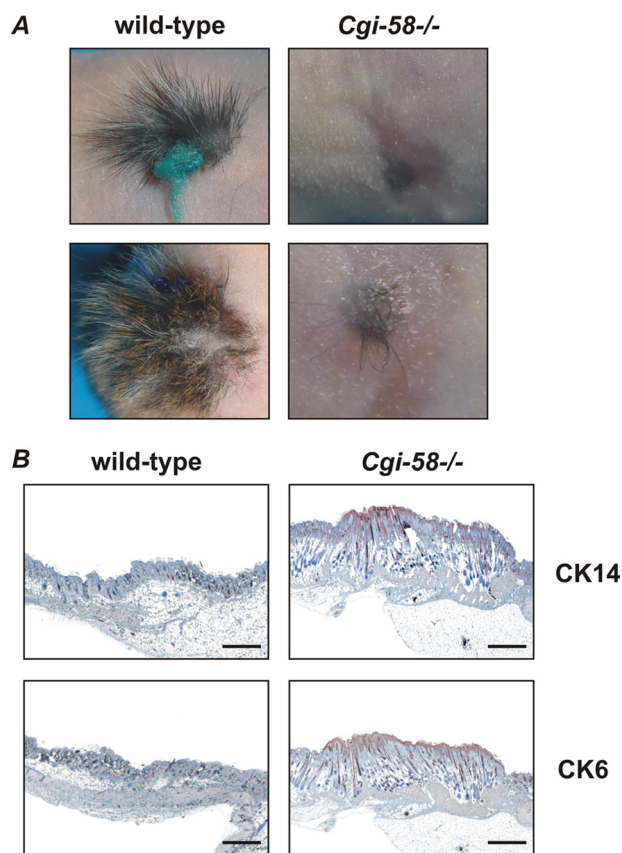


FIGURE 6. Impaired hair growth and skin development of *Cgi-58*^{-/-} skins grafted onto nude mice. A and B, wild-type and *Cgi-58*^{-/-} skins were grafted onto nude mice and photographed after 3 weeks (A) or sections of grafted skin were stained with antibodies specific for cytokeratin 14 (CK14) or cytokeratin 6 (CK6) and analyzed by light microscopy (B). Results are representative for four independent transplantation experiments. Scale bars represent 500 μ m.

in these processes will thus require the characterization of conditional CGI-58 knock-out mice.

Newborn *Cgi-58*^{-/-} mice exhibited an increased hepatic TG content compared with wild-type mice suggesting a role of CGI-58 in the regulation of the hepatic fat content. Hepatosteatosis was associated with markedly lower TG hydrolase activities in liver lysates of CGI-58-deficient mice than those of wild-type animals. Hepatic TG levels and lipolytic activities were similar to those in newborn *Atgl*^{-/-} mice. In contrast to *Atgl*^{-/-} liver samples, however, the TG hydrolase activities of *Cgi-58*^{-/-} liver samples could be completely restored by the addition of recombinant GST-CGI-58. These findings indicate that the lipolytic defect originates predominantly from reduced ATGL activity in the liver rather than the action of a non-ATGL liver lipase. The results are also consistent with data showing that CGI-58 affects cellular TG catabolism and the synthesis of very low density lipoproteins in cultured hepatoma cell lines (38, 39).

In addition to its function in activating ATGL, CGI-58 was shown to operate as a lysophosphatidic acid acyltransferase (LPAAT) *in vitro* (25, 26). This finding correlates with previous studies showing that fibroblasts of patients affected with NLSDI exhibit a defect in the remodeling of TG to glycerophospholipids (31). Whether LPAAT activity is impaired in tissues

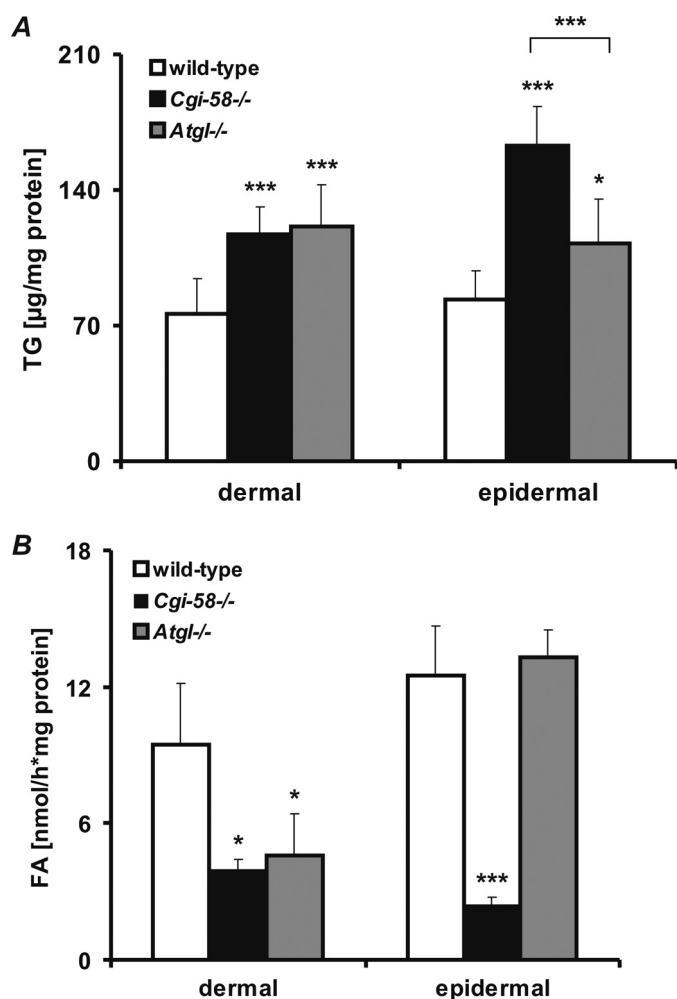


FIGURE 7. Dermis and epidermis of *Cgi-58*^{-/-} mice accumulate TG and exhibit impaired TG hydrolase activity. *A*, skins of newborn wild-type, *Cgi-58*^{-/-}, and *Atgl*^{-/-} mice were surgically removed. Epidermis was separated from dermis and epidermal and dermal lipids were extracted for determination of TG content. *B*, TG hydrolase activities of epidermal and dermal lysates from newborn wild-type, *Cgi-58*^{-/-}, and *Atgl*^{-/-} mice were determined using phospholipid-emulsified triolein substrate, containing [9,10-³H]triolein as tracer. Release of radiolabeled FA was determined by liquid scintillation counting. Data are means ± S.D. (*n* = 6–8) and representative for three independent experiments. Statistical significance was determined by the two-tailed Student's *t* test (*, *p* < 0.05; ***, *p* < 0.001).

and cells of NLSDI patients has not been directly examined. However, *CGI-58* mutations causing NLSDI exhibited normal LPAAT activity *in vitro* (25). This finding questions a causative role for defective *CGI-58*-mediated LPAAT activity in NLSDI development. In our animal model for NLSDI, total LPAAT activity was unaffected in whole liver or skin lysates of *CGI-58*-deficient mice (data not shown). A causal relationship between LPAAT deficiency and excessive neutral lipid accumulation in *CGI-58*-deficient mice and humans also seems unlikely in a metabolic context. LPAAT activity is required for the formation of phosphatidic acid, which is a prerequisite for the synthesis of both TG and glycerophospholipids (40, 41). Consistent with defective TG synthesis, patients that lack specific isoforms of LPAAT activity (e.g. 1-acylglycerol-3-phosphate *O*-acyltransferase 2 deficiency) suffer from the absence of TG in cells and develop severe lipodystrophy (42, 43), whereas *Cgi-58*^{-/-} mice and patients with NLSDI are characterized by excessive

lipid deposition in multiple tissues. However, it is conceivable that this activity is specific to a certain cellular compartment (e.g. LD or lamellar bodies) and/or substrate (e.g. ω -OH-ceramide species, retinol, etc.) and therefore masked by the total cellular LPAAT activity.

The severe skin defect in *Cgi-58*^{-/-} mice originates from an ATGL-independent mechanism, because mice and humans lacking ATGL activity do not develop ichthyosis (14, 15). Transplantation experiments of *CGI-58*-deficient skin onto nude mice proved that the defect was inherent to the skin and not the result of systemic metabolic alterations. To illuminate the function of *CGI-58* in the skin, we analyzed its involvement in TG metabolism. In the dermis, the TG content was increased and TG hydrolase activity was decreased to a similar extent in *Cgi-58*^{-/-} and *Atgl*^{-/-} mice compared with wild-type samples, consistent with the view that dermal TG catabolism is predominantly mediated by ATGL. In contrast, TG content in the epidermis was much higher in *Cgi-58*^{-/-} mice than in *Atgl*^{-/-} and wild-type animals. Conversely, TG hydrolase activity was substantially lower in *Cgi-58*^{-/-} epidermal lysates than in wild-type and *Atgl*^{-/-} lysates. Defective epidermal lipolysis in the absence of *CGI-58* led to an impaired TG turnover and FA release from cellular LD, as evident from pulse-chase experiments. These findings are consistent with the observation that NLSDI patients lacking functional *CGI-58* accumulate TG-enriched LD in the epidermis of their skin (27). Considering that *CGI-58* itself lacks TG hydrolase activity, we conclude that in addition to ATGL a lipase in the skin exists, which hydrolyzes epidermal TG. The results also imply that analogously to ATGL, this currently unknown enzyme requires *CGI-58* for full activity. The existence of at least two separate neutral skin lipases, one specific for short chain TG and the other specific for long chain TG, was predicted earlier (44). A recent study surveyed human genes implicated in epidermal barrier function and presented a list of several potential candidates for the postulated epidermal TG lipase(s) on the basis of microarray expression profiling (45). The list included patatin protein family members, lipase-like genes, esterase/carboxyl esterases, and α/β -hydrolase domain containing protein family members. Whether any of these candidates are *CGI-58*-activated TG hydrolases with substrate specificity for long chain FA remains to be determined.

This study demonstrates a direct link between epidermal TG catabolism and the formation of a functional CLE. The formation of the CLE involves the covalent binding of ω -OH ceramides to the protein mantle of corneocytes (46). A multiple step remodeling pathway of the ceramide ligand precedes the lipid-protein bonding. According to the current concept, ω -OH-ceramides derive from the ω -hydroxylation of very long chain FA (presumably by a cytochrome P450-mediated process) and their subsequent amide formation with sphingol, a precursor of ceramides (36). ω -OH-ceramides are then acylated by esterification of the ω -OH group with oleic or linoleic acid. The resulting acylceramides are glycosylated by glucosylceramide synthase and bonded to the carboxyl termini of involucrin, by a process that involves several enzymes, including transglutaminase-1 and β -glucocerebrosidase (36). Our data show that in

CGI-58 Deficit Impairs Hepatic and Epidermal TG Catabolism

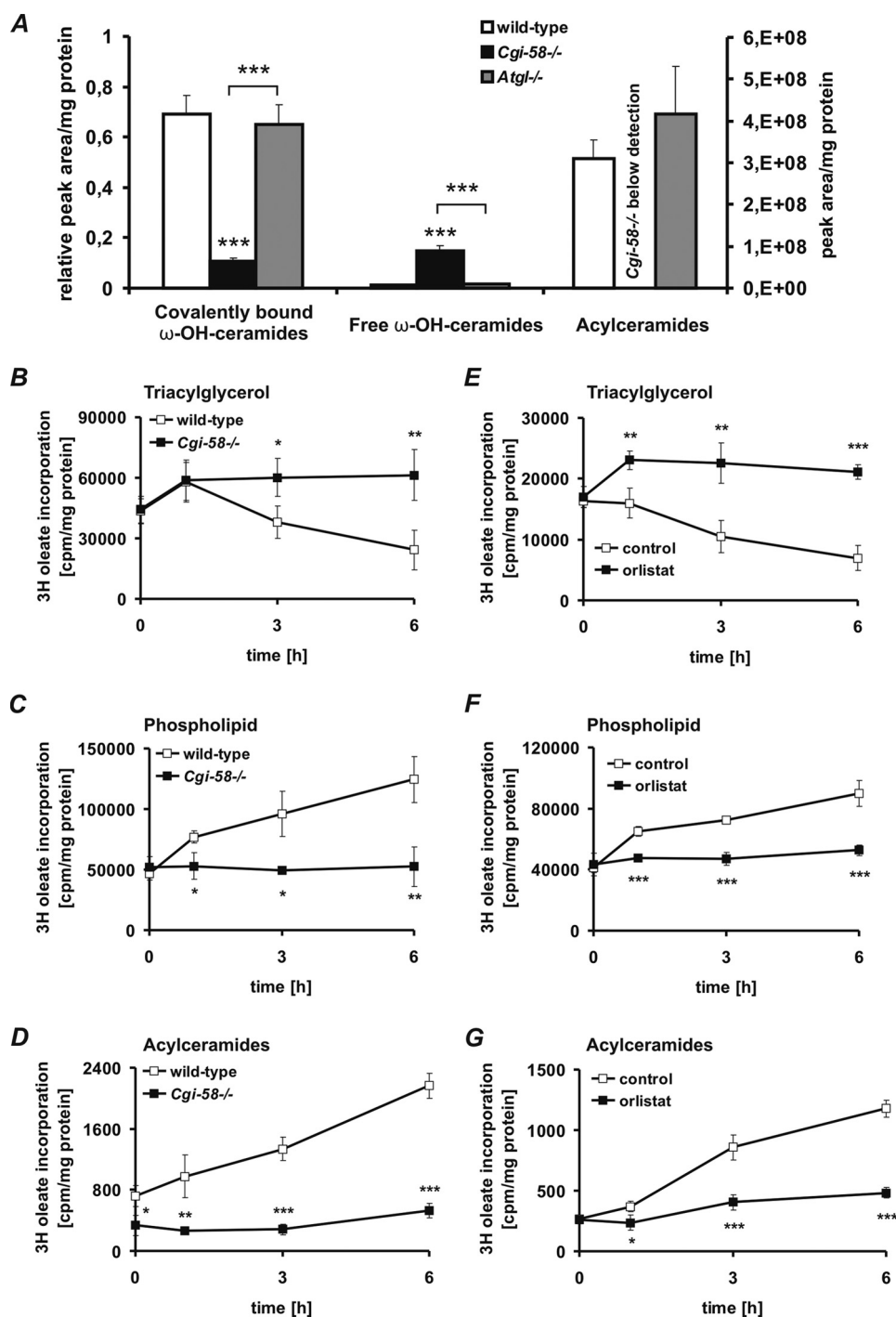


FIGURE 8. Acylceramide formation is impaired in *Cgi-58*^{-/-} epidermis. A, epidermal lipids were extracted from newborn wild-type, *Cgi-58*^{-/-}, and *Atgl*^{-/-} mice. Free ω -OH ceramides and acylceramides were analyzed by UPLC-MSMS. Covalently bound ω -OH ceramides of the extracted epidermises were released by mild alkaline hydrolysis and analyzed by UPLC-MSMS. Peak areas of ceramide species were combined and normalized to epidermal protein content. B–D, epidermal sheets of newborn wild-type and *Cgi-58*^{-/-} mice were incubated in DMEM containing 400 μ M oleate and [9,10-³H]oleate as tracer. After 5 h, epidermal sheets were washed and chased in DMEM for 6 h. At various time points, total lipids of epidermal sheets were extracted. Neutral lipids were separated by TLC using hexane/diethyl ether/glacial acetic acid (70:29:1) as solvent system, and radioactivity in the TG fraction was determined by liquid scintillation counting (B). Polar lipids were separated twice by TLC using chloroform/methanol/acetic acid (190:9:1) as solvent system. Radioactivity in the phospholipid (C) and acylceramide (D) fraction was determined by liquid scintillation counting. E–G, wild-type epidermal sheets were incubated in DMEM containing 400 μ M oleate and [9,10-³H]oleate as tracer. After 5 h, epidermal sheets were washed and chased in DMEM in the presence or absence of orlistat (20 μ M). At various time points, radioactivity in TG (E), phospholipid (F), and acylceramide (G) fractions was determined as described above. Data are means \pm S.D. ($n = 3-6$) and representative for three independent experiments. Statistical significance was determined by the two-tailed Student's *t* test (*, $p < 0.05$; **, $p < 0.01$; ***, $p < 0.001$).

the absence of CGI-58, FA are trapped in cellular TG stores and not transferred to ω -OH-ceramides (and phospholipids). Accordingly, the epidermal concentration of acylceramides and protein-bound ceramides was extremely low or undetectable, whereas unbound ω -OH-ceramide levels were elevated. Inhibition of epidermal TG lipases by the nonspecific inhibitor orlistat also prevented acylceramide formation suggesting that the hydrolytic degradation of the epidermal TG pool is a requirement for the subsequent acylceramide synthesis.

The concept that FA for acylceramide formation have to cycle through esterification (TG synthesis) and re-hydrolysis (TG degradation by lipases) is also supported by induced mutant mice that lack the principal enzyme in epidermal TG synthesis, DGAT2 (acyl-CoA: diacylglycerolacyltransferase-2). DGAT2-deficient mice lacking epidermal TG synthesis also exhibited drastically reduced acylceramide concentrations in the skin (47). Yet phospholipid levels were not affected in both the DGAT2- and CGI-58-deficient mouse model. Interestingly, DGAT2-deficient animals developed a skin phenotype very similar to that observed in CGI-58-deficient mice and also died soon after birth.

In summary, our study assigns an essential role to CGI-58 in TG catabolism. CGI-58 deficiency leads to deranged lipid accumulation in the skin and liver suggesting that CGI-58-activated fat degradation plays an important role in hepatic TG homeostasis. Additionally, the crucial role of epidermal TG catabolism for acylceramide synthesis provided novel insights into the molecular mechanisms involved in ichthyosis development of NLSID patients. The pharmacological activation of CGI-58-mediated TG catabolism in the skin and liver might provide a novel molecular target for the treatment of ichthyosiform skin disorders and hepatic steatosis, respectively.

Acknowledgments—We thank Dr. D. L. Brasaemle for kindly providing the rabbit polyclonal CGI-58 antiserum. We thank Dr. J. Wojciechowski for blastocyst injections, Mag. B. Juritsch and A. Hermann for their excellent technical assistance, and Dr. E. Zechner and Mag. C. Lanschützer for critically reading the manuscript.

REFERENCES

- Dorfman, M. L., Hershko, C., Eisenberg, S., and Sagher, F. (1974) *Arch. Dermatol.* **110**, 261–266
- Chanarin, I., Patel, A., Slavina, G., Wills, E. J., Andrews, T. M., and Stewart, G. (1975) *Br. Med. J.* **1**, 553–555
- Igal, R. A., Rhoads, J. M., and Coleman, R. A. (1997) *J. Pediatr. Gastroenterol. Nutr.* **25**, 541–547
- Kahn, B. B., and Flier, J. S. (2000) *J. Clin. Invest.* **106**, 473–481
- Spiegelman, B. M., and Flier, J. S. (2001) *Cell* **104**, 531–543
- Qatanani, M., and Lazar, M. A. (2007) *Genes Dev.* **21**, 1443–1455
- Jenkins, C. M., Mancuso, D. J., Yan, W., Sims, H. F., Gibson, B., and Gross, R. W. (2004) *J. Biol. Chem.* **279**, 48968–48975
- Villena, J. A., Roy, S., Sarkadi-Nagy, E., Kim, K. H., and Sul, H. S. (2004) *J. Biol. Chem.* **279**, 47066–47075
- Zimmermann, R., Strauss, J. G., Haemmerle, G., Schoiswohl, G., Birner-Gruenberger, R., Riederer, M., Lass, A., Neuberger, G., Eisenhaber, F., Hermetter, A., and Zechner, R. (2004) *Science* **306**, 1383–1386
- Holm, C., Kirchgessner, T. G., Svenson, K. L., Fredrikson, G., Nilsson, S., Miller, C. G., Shively, J. E., Heinzmann, C., Sparkes, R. S., Mohandas, T., et al. (1988) *Science* **241**, 1503–1506
- Raben, D. M., and Baldassare, J. J. (2005) *Trends Endocrinol. Metab.* **16**, 35–36
- Osuga, J., Ishibashi, S., Oka, T., Yagyu, H., Tozawa, R., Fujimoto, A., Shionoiri, F., Yahagi, N., Kraemer, F. B., Tsutsumi, O., and Yamada, N. (2000) *Proc. Natl. Acad. Sci. U.S.A.* **97**, 787–792
- Haemmerle, G., Zimmermann, R., Hayn, M., Theussl, C., Waeg, G., Wagner, E., Sattler, W., Magin, T. M., Wagner, E. F., and Zechner, R. (2002) *J. Biol. Chem.* **277**, 4806–4815
- Haemmerle, G., Lass, A., Zimmermann, R., Gorkiewicz, G., Meyer, C., Rozman, J., Heldmaier, G., Maier, R., Theussl, C., Eder, S., Kratky, D., Wagner, E. F., Klingenspor, M., Hoefler, G., and Zechner, R. (2006) *Science* **312**, 734–737
- Fischer, J., Lefèvre, C., Morava, E., Mussini, J. M., Laforêt, P., Negre-Salvayre, A., Lathrop, M., and Salvayre, R. (2007) *Nat. Genet.* **39**, 28–30
- Hirano, K., Ikeda, Y., Zaima, N., Sakata, Y., and Matsumiya, G. (2008) *N. Engl. J. Med.* **359**, 2396–2398
- Lass, A., Zimmermann, R., Haemmerle, G., Riederer, M., Schoiswohl, G., Schweiger, M., Kienesberger, P., Strauss, J. G., Gorkiewicz, G., and Zechner, R. (2006) *Cell Metab.* **3**, 309–319
- Yamaguchi, T., Omatsu, N., Morimoto, E., Nakashima, H., Ueno, K., Tanaka, T., Satouchi, K., Hirose, F., and Osumi, T. (2007) *J. Lipid Res.* **48**, 1078–1089
- Lefèvre, C., Jobard, F., Caux, F., Bouadjar, B., Karaduman, A., Heilig, R., Lakhdar, H., Wollenberg, A., Verret, J. L., Weissenbach, J., Ozgüc, M., Lathrop, M., Prud'homme, J. F., and Fischer, J. (2001) *Am. J. Hum. Genet.* **69**, 1002–1012
- Subramanian, V., Rothenberg, A., Gomez, C., Cohen, A. W., Garcia, A., Bhattacharyya, S., Shapiro, L., Dolios, G., Wang, R., Lisanti, M. P., and Brasaemle, D. L. (2004) *J. Biol. Chem.* **279**, 42062–42071
- Yamaguchi, T., Omatsu, N., Matsushita, S., and Osumi, T. (2004) *J. Biol. Chem.* **279**, 30490–30497
- Granneman, J. G., Moore, H. P., Mottillo, E. P., and Zhu, Z. (2009) *J. Biol. Chem.* **284**, 3049–3057
- Granneman, J. G., Moore, H. P., Granneman, R. L., Greenberg, A. S., Obin, M. S., and Zhu, Z. (2007) *J. Biol. Chem.* **282**, 5726–5735
- Granneman, J. G., Moore, H. P., Krishnamoorthy, R., and Rathod, M. (2009) *J. Biol. Chem.* **284**, 34538–34544
- Ghosh, A. K., Ramakrishnan, G., Chandramohan, C., and Rajasekharan, R. (2008) *J. Biol. Chem.* **283**, 24525–24533
- Montero-Moran, G., Caviglia, J. M., McMahon, D., Rothenberg, A., Subramanian, V., Xu, Z., Lara-Gonzalez, S., Storch, J., Carman, G. M., and Brasaemle, D. L. (2010) *J. Lipid Res.*, in press
- Akiyama, M., Sawamura, D., Nomura, Y., Sugawara, M., and Shimizu, H. (2003) *J. Invest. Dermatol.* **121**, 1029–1034
- Taniguchi, M., Sanbo, M., Watanabe, S., Naruse, I., Mishina, M., and Yagi, T. (1998) *Nucleic Acids Res.* **26**, 679–680
- Ausubel, F. M., Brent, R., Kingston, R. E., Moore, D. D., Seidman, J. G., Smith, J. A., and Struhl, K. (eds) (2004) *Current Protocols in Molecular Biology*, Vol. 2, pp. 10.2A.1–10.2A.27, John Wiley & Sons, Inc., New York
- Wertz, P. W., Miethke, M. C., Long, S. A., Strauss, J. S., and Downing, D. T. (1985) *J. Invest. Dermatol.* **84**, 410–412
- Igal, R. A., and Coleman, R. A. (1996) *J. Biol. Chem.* **271**, 16644–16651
- McMahon, A., Butovich, I. A., Mata, N. L., Klein, M., Ritter, R., 3rd, Richardson, J., Birch, D. G., Edwards, A. O., and Kedzierski, W. (2007) *Mol. Vis.* **13**, 258–272
- Jordans, G. H. (1953) *Acta Med. Scand.* **145**, 419–423
- Navarro, J. M., Casatorres, J., and Jorcano, J. L. (1995) *J. Biol. Chem.* **270**, 21362–21367
- Andreassi, S. T., Hamoen, K. E., Yarmush, M. L., and Morgan, J. R. (2001) *FASEB J.* **15**, 898–906
- Uchida, Y., and Holleran, W. M. (2008) *J. Dermatol. Sci.* **51**, 77–87
- Guercioli, R. (1997) *Int. J. Obes. Relat. Metab. Disord.* **21**, Suppl. 3, 12–23
- Brown, J. M., Chung, S., Das, A., Shelness, G. S., Rudel, L. L., and Yu, L. (2007) *J. Lipid Res.* **48**, 2295–2305
- Caviglia, J. M., Sparks, J. D., Toraskar, N., Brinker, A. M., Yin, T. C., Dixon, J. L., and Brasaemle, D. L. (2009) *Biochim. Biophys. Acta* **1791**, 198–205
- Péterfy, M., Phan, J., Xu, P., and Reue, K. (2001) *Nat. Genet.* **27**, 121–124
- Han, G. S., Wu, W. I., and Carman, G. M. (2006) *J. Biol. Chem.* **281**, 9210–9218
- Agarwal, A. K., Arioglu, E., De Almeida, S., Akkoc, N., Taylor, S. I., Bowcock, A. M., Barnes, R. I., and Garg, A. (2002) *Nat. Genet.* **31**, 21–23
- Garg, A., and Agarwal, A. K. (2009) *Biochim. Biophys. Acta* **1791**, 507–513
- Hilaire, N., Salvayre, R., Thiers, J. C., Bonnafé, M. J., and Nègre-Salvayre, A. (1995) *J. Biol. Chem.* **270**, 27027–27034
- Toulza, E., Mattiuzzo, N. R., Galliano, M. F., Jonca, N., Dossat, C., Jacob, D., de Daruvar, A., Wincker, P., Serre, G., and Guerrin, M. (2007) *Genome Biol.* **8**, R107
- Candi, E., Schmidt, R., and Melino, G. (2005) *Nat. Rev. Mol. Cell Biol.* **6**, 328–340
- Stone, S. J., Myers, H. M., Watkins, S. M., Brown, B. E., Feingold, K. R., Elias, P. M., and Farese, R. V., Jr. (2004) *J. Biol. Chem.* **279**, 11767–11776